

Axial patterning of the pentaradial adult echinoderm body plan

Sharon B. Minsuk · F. Rudolf Turner ·
Mary E. Andrews · Rudolf A. Raff

Received: 13 June 2008 / Accepted: 2 January 2009 / Published online: 3 February 2009
© Springer-Verlag 2009

Abstract Adult echinoderms possess a highly diverged, pentaradial body plan. Developmental mechanisms underlying this body plan are completely unknown, but are critical in understanding how echinoderm pentamery evolved from bilateral ancestors. These mechanisms are difficult to study in indirect-developing species; in this study, we use the direct-developing sea urchin *Heliocidaris erythrogramma*, whose accelerated adult development can be perturbed by NiCl₂. We introduce a new nomenclature for the adult echinoderm axes to facilitate discussion of the radially symmetric body plan and the events required to pattern it. In sea urchins, the adult oral–aboral axis is often conflated with the long axes of the five rays; we identify these as distinct body axes, the proximodistal (PD). In addition, we define a circular axis, the circumoral (CO), along which the division into five sectors occurs. In NiCl₂-treated larvae, aspects of normal PD pattern were retained, but CO pattern was abolished. Milder treatments resulted in relatively normal juveniles ranging from biradial to decaradial. NiCl₂ treatment had no effect either on mesodermal morphology or on the ectodermal gene expression response

to an inductive mesodermal signal. This suggests that the mesoderm does not mediate the disruption of CO patterning by NiCl₂. In contrast, mesodermal signaling may explain the presence of PD pattern in treated larvae. However, variations in appendage pattern suggest that ectodermal signals are also required. We conclude that CO patterning in both germ layers is dependent on ectodermal events and PD patterning is controlled by mutual ectoderm–mesoderm signaling.

Keywords Radial symmetry · Mesoderm–ectoderm signaling · Axial homologies · Echinoderms · Body plan patterning

Introduction

The pentaradial adult echinoderm body—a major evolutionary novelty—is divided into five sectors (the rays or radii), arranged around an axis of radial symmetry, the oral–aboral (OA) axis. As larvae, however, echinoderms are bilaterally symmetrical; the radial body plan arises only later, in presumptive adult tissues that establish new axes, supplanting the larval ones (MacBride 1903; Hyman 1955; Okazaki 1975; Minsuk et al. 2005). Furthermore, the closest relatives of echinoderms, the hemichordates, have similar larvae but undergo no axial remodeling, remaining bilaterally symmetric throughout their lives (Hyman 1959; Hadfield 1975; Peterson et al. 1999; Urata and Yamaguchi 2004). Thus, echinoderm development is a striking example not only of body plan transformation during the life of an individual, but also of the evolutionary transformation of development from that of their bilaterally symmetric ancestors. But the developmental mechanisms underlying these transformations are not easily accessible to study in

Communicated by N. Satoh

S. B. Minsuk (✉) · F. R. Turner · M. E. Andrews · R. A. Raff
Department of Biology and Indiana Molecular Biology Institute,
Indiana University,
Bloomington, IN 47405, USA
e-mail: sharon@sharonminsuk.com

Present address:

S. B. Minsuk
Department of Biology, Merritt College,
Oakland, CA 94619, USA

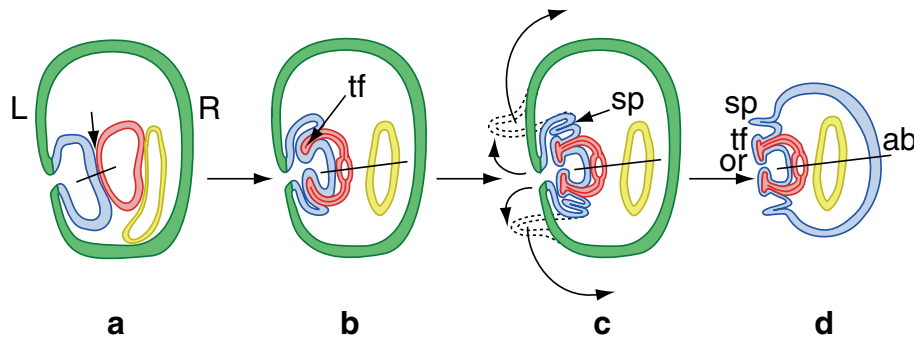


Fig. 1 Simplified diagram of adult body plan development and metamorphosis in *H. erythrogramma*. Green larval ectoderm, blue vestibular ectoderm, red coelomic mesoderm, yellow endoderm, black bar adult OA axis. **a** The adult rudiment forms where the vestibular ectoderm meets the left coelom (arrow). **b** Formation of tube foot

primordia. **c** Mature tube feet and adult spine primordia. Juvenile spines also form around this time but have been omitted for clarity (see Fig. 3). The vestibular ectoderm will evert and wrap around the internal organs as shown. **d** The resulting juvenile. *L* larval left, *R* larval right, *ab* aboral, *or* oral, *sp* adult spine, *tf* tube foot

the commonly studied indirect-developing species because they act only after a lengthy feeding larval stage. We have begun to elucidate these mechanisms using a more suitable model, the direct-developing sea urchin *Heliocidaris erythrogramma* (Minsuk and Raff 2002; Minsuk et al. 2005), which does not feed and which initiates adult development after only a day, before even the reduced larval features of this species (Williams and Anderson 1975; Emler 1995) have completed their development. Adult development in *H. erythrogramma*, unlike its larval development, is conserved with respect to that of other sea urchins (Williams and Anderson 1975; Haag and Raff 1998; Ferkowicz and Raff 2001) and, therefore, provides an accessible model for the development of the echinoderm adult body plan.

Sea urchin adult development begins with the establishment of left–right larval asymmetry (McCain and McClay 1994; Summers et al. 1996; Aihara and Amemiya 2001; Duboc et al. 2005; Minsuk et al. 2005). In most sea urchins, this is followed by the specification of the coelomic mesoderm and the vestibular (presumptive adult) ectoderm on the left side of the larval body, which meet and form the two-layered adult rudiment. The OA axis is perpendicular to these layers, and the adult body plan will be organized around it (Fig. 1a, b) (MacBride 1903; Hyman 1955; Minsuk and Raff 2002). In *H. erythrogramma*, the vestibular/larval (V/L) ectodermal boundary is set up by intraectodermal signals (Minsuk et al. 2005; Minsuk and Raff 2005), and the vestibular ectoderm then invaginates to form the vestibule cavity within which the adult will later develop (Haag and Raff 1998). The left coelom may play a complementary or redundant role in regulating early vestibule formation (Minsuk et al. 2005). We know that the left coelom provides an inductive signal required for further adult ectodermal development (Minsuk and Raff 2002), but the mechanisms that pattern the adult body plan are unknown.

The center of the vestibule floor is the future site of the adult mouth and is, therefore, the oral end of the adult OA axis (Fig. 1). To best describe the adult echinoderm body plan, we use a polar coordinate system centered on the mouth (Fig. 2). The OA axis is the axis of coelomic stacking (David and Mooi 1998; Peterson et al. 2000). The rays extend outward from the mouth, expressing proximodistal (PD) pattern in the arrangement of appendages (tube feet and spines) along each ray. The rays are arranged in a ring around the mouth; there are standard systems for naming the individual rays (Paul and Smith 1984), but no terminology to identify the path around this ring as a direction of patterning. We define this circular path as the circumoral (CO) axis. CO pattern includes the segmentation of the ring into five sectors and the edge-to-edge or mediolateral arrangement of appendages within each sector. In sea urchins (Fig. 2), this coordinate system gets folded

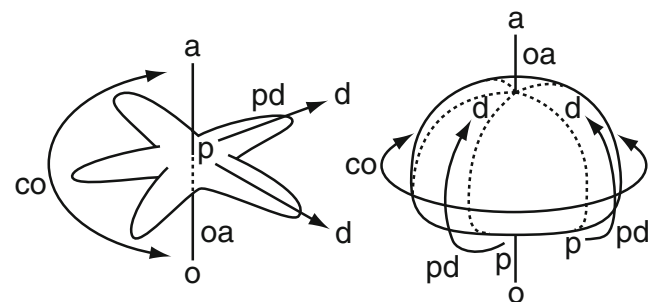


Fig. 2 Axial orientations in echinoderms. In starfish (left), the proximodistal axes extend outward along the arms, perpendicular to the OA axis. The circumoral axis sweeps around the circle within each arm and from one arm to the next. In sea urchins (right), the same proximodistal axes are wrapped around the body surface like longitude lines. These are homologous to the starfish rays and thus are distinct from the OA axis despite extending from the oral toward the aboral pole. The circumoral axis rings the body like latitude lines. *oa* oral–aboral axis, *pd* proximodistal axes, *co* circumoral axis, *o* oral pole, *a* aboral pole, *p* proximal pole, *d* distal poles

up around the surface of the animal during metamorphosis so that the PD axes now converge toward the aboral pole, like the longitude lines on a globe. It is important to note that the PD axes remain distinct from the OA axis, since the PD axis of each ray is perpendicular to the OA axis within the developing rudiment. The CO axis circles the animal like latitude lines on a globe.

The first morphological expression of these patterns is the development of five cylindrical lobes protruding from the hydrocoel (a subdivision of the left coelom), in a CO arrangement (Ferkowicz and Raff 2001). The vestibular ectoderm then provides a corresponding outer layer to each growing lobe, forming the first five tube feet or primary podia (Fig. 1b). Spine primordia then arise, expressing both PD and CO pattern. Two concentric zones produce morphologically distinct spines containing characteristic skeletons secreted by mesenchyme cells (Williams and Anderson 1975)—“adult” or definitive spines in the proximal zone together with the tube feet, and “juvenile” spines in the distal zone. Within each zone, these spines express the fivefold CO periodicity of the adult body plan. At metamorphosis, the vestibule will evert so that the vestibular ectoderm encloses the internal organs. The larval ectoderm is largely excluded; thus, the lip of the vestibular opening comes to lie near the opposite (aboral) end of the juvenile and the vestibular ectoderm becomes the juvenile epidermis (Fig. 1c–d). Additional juvenile spines develop further aborally in an irregular arrangement; these develop outside the rudiment and vestibule, in separate larval ectodermal invaginations (our unpublished observations), and are, therefore, extraxial structures (David and Mooi 1998), meaning that they are not part of the pentaradially patterned portion of the adult body.

The patterning mechanisms underlying these events have never been addressed in any echinoderm. The rudiment must be subdivided into five sectors; angular positions within each sector must be specified (e.g., the alternating tube feet and adult spines); and unique ray identities must be established (Paul and Smith 1984). Likewise, proximal and distal territories (e.g., adult vs. juvenile spines) must be specified. We ask what determines the size and number of repeated units around the OA axis, what determines the locations and identities of organ primordia as they form at different CO and PD coordinates, and whether signals between the tissues contribute to patterning the adult body plan.

In this study, we address these questions by means of NiCl₂ treatment of embryos. In indirect-developing sea urchins, NiCl₂ ventralizes the pluteus larva by interfering with larval axial patterning in the ectoderm (Hardin et al. 1992). In those species, NiCl₂-treated embryos arrest before the coelomic mesoderm or vestibular ectoderm develop, so its effect on adult patterning cannot be measured. Previ-

ously (Minsuk and Raff 2005), we described the response of *H. erythrogramma* larval and vestibular ectoderm to the same treatment and used it to compare larval axial patterning mechanisms in the two developmental modes. However, because *H. erythrogramma* undergoes precocious adult rudiment development without having to pass through a feeding pluteus stage, adult development begins while larval axial patterning events are still taking place, allowing us to use NiCl₂ treatment to study adult axial patterning as well. Thus, in this study, *H. erythrogramma*'s unusual developmental chronology has made it possible to examine adult developmental mechanisms for the first time.

In normal *H. erythrogramma* embryos, the vestibule invaginates on the left side and the V/L boundary forms a contracting circular lip (Emlet 1995; Haag and Raff 1998; Minsuk et al. 2005). In contrast, as shown in our previous study (Minsuk and Raff 2005), NiCl₂-treated embryos produce a sinistralized larva surrounded by a circumferential band of vestibular ectoderm, bounded animally and vegetally by larval ectoderm, and thus have two ectopic V/L boundaries, expressed circumferentially. These ectopic boundaries contract, pinching off animal and vegetal lobes which detach, leaving only the hourglass-shaped larval midsection, enclosed entirely by vestibular ectoderm (Minsuk and Raff 2005) and containing the bulk of the endodermal and mesodermal tissues. This larval midsection is the starting point for the present investigation of adult development.

Normal tube feet and spines subsequently develop. In this study, we describe the pattern of appendage development in NiCl₂-treated larvae and investigate the patterning mechanisms underlying it. Based on our results, we have developed the first rudimentary model of patterning events underlying echinoderm pentaradial symmetry. Understanding these events is critical to understanding the evolutionary origin of the echinoderm adult body plan.

Materials and methods

Gametes of *H. erythrogramma* were obtained from adults injected with 0.55 M KCl. Embryos were cultured at 19–25°C in NiCl₂ solutions prepared in 0.45 μm Millipore filtered sea water (FSW). After treatment, larvae were transferred back into FSW with several rinses. Dead or dying embryos were removed from the dishes.

The experiments in this paper used the same specimens generated in a previously published, concurrent study (Minsuk and Raff 2005), which examined the effects of NiCl₂ on larval ectoderm development, including extensive characterization of dose and timing responses. In that study, treatment with a moderate NiCl₂ concentration (2–10 μM) during a NiCl₂-sensitive critical period (through the

midgastrula stage) caused a specific, uniform, predictable phenotype in which larval ectoderm was completely sinistralized, expressing a left-side identity around the entire circumference. Lower concentrations produced variable degrees of partial sinistralization, whereas higher concentrations produced nonspecific defects and inhibition of development.

That study examined larval ectoderm development through completion of vestibular ectoderm, prior to the appearance of any adult features (tube feet, spines, adult skeleton). The present study examines the subsequent development of larvae from the 2- to 5- μ M treatments (exhibiting complete sinistralization and no additional defects) in order to examine adult phenotypes. In additional experiments, embryos were treated later, at very early gastrula stages (the end of the critical period), to generate milder effects. We also revisited the larval stages in order to observe early rudiment mesodermal morphology and vestibular ectodermal gene expression, the precursors of adult development.

Larvae are competent to metamorphose at 3.5 to 4 days, but do not always do so on their own under laboratory conditions. In order to trigger metamorphosis in competent (mildly treated or untreated) larvae and examine the resulting juveniles, we added small sprigs of live coralline algae (a natural trigger) to the culture dishes.

Live specimens were photographed on a Zeiss stereoscope under epi-illumination or on a Zeiss Axioplan

compound microscope (Carl Zeiss, Thornwood, NY) either under bright field or under polarized light to view the birefringent CaCO_3 skeleton. Other specimens were fixed in 2% paraformaldehyde in FSW, embedded in Paraplast, and sectioned. We viewed 10- μ m sections under differential interference contrast (DIC) optics after staining with toluidine blue and eosin, and 5- μ m sections in bright and dark field illumination after radioactive in situ hybridization with a probe to *HeARS* (arylsulfatase, an ectodermal marker) as previously described (Angerer and Angerer 1991; Haag and Raff 1998). Additional fixed specimens were critical point dried, sputter coated, and viewed by scanning electron microscopy (SEM).

Results

Normal juveniles express a pentaradial pattern with concentric proximal and distal zones

In newly metamorphosed, untreated control juveniles, the center of the polar coordinate system and the site of future mouth formation can be found at the oral end of the OA axis (center of Fig. 3c), surrounded by two concentric zones of spines, “adult” and “juvenile” spines (Fig. 3a). The adult spines, in the inner or proximal zone, are organized in five triplets alternating with the tube feet; the juvenile spines, in

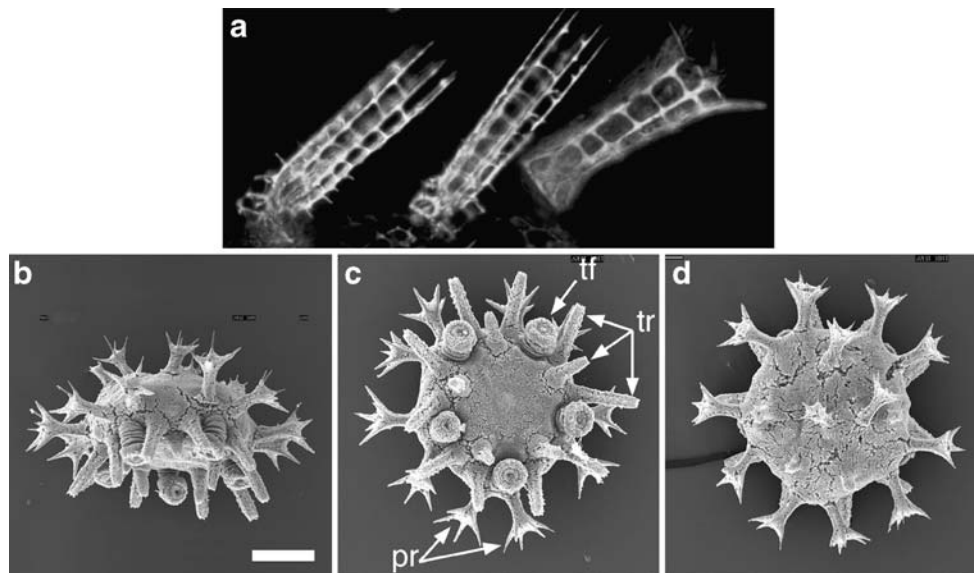


Fig. 3 Normal juvenile morphology. **a** *H. erythrogramma* spines viewed live under polarized light at 5 days, revealing the skeleton. Tips of spines point toward the upper right. Adult spines, more proximal (*left* and *center*), have blunt tips that later develop a tapered point; juvenile spines, more distal (*right*), have splayed, claw-like tips. **b–d** Newly metamorphosed juveniles (approximately 4 days) viewed by SEM. **b** Lateral view: oral side down with adult spines and tube feet; aboral side up with juvenile spines. **c** Oral view, displaying

pentaradial symmetry: site of future adult mouth is in the center, surrounded by five tube feet (*tf*) and five adult spine triplets (*tr*) proximally; these are surrounded in turn by an equatorial ring of juvenile spine pairs (*pr*) distally, each pair associated with one tube foot. **d** Aboral view: five pairs of juvenile spines ring the equator. Additional juvenile spines project upward (toward the viewer) from the aboral surface. Bar=200 μ m

the outer or distal zone, are arranged in five pairs, each just distal to one of the five tube feet (Fig. 3b, c). Thus, the proximal zone (tube feet and adult spines) surrounds the oral pole, and the distal zone (juvenile spines) rings the equator. Additional, extraxial juvenile spines are located further distally, in the aboral half of the body (Fig. 3d).

NiCl₂-treated larvae develop normal, but abnormally arranged, adult appendages

In contrast to the invaginated vestibular ectodermal cavity of untreated larvae (Fig. 1a), sinistralized larvae are surrounded by a circumferential band of vestibular ectoderm (Fig. 5g–h). This is initially flanked by animal (*al* in Figs. 4a and 6b) and vegetal lobes of larval ectoderm,

which detach with variable timing, ultimately leaving only the hourglass-shaped vestibular midsection in which adult development occurs. After detachment, the shape of the midsection resembles that of the schematic diagrams in Fig. 8b–d.

Tube foot development (Fig. 4a) began at 40–45 h postfertilization (a delay of about 10 h compared to untreated larvae; Fig. 1b). Most tube feet developed to maturity, becoming motile and forming suckers (Fig. 4d) with normal pigmentation, and finally developing normal internal skeletal rings (Fig. 4b, c). However, they were somewhat variable in diameter (Fig. 4b, c) and usually did not adhere to the dish bottom. NiCl₂-treated “juveniles” never walked or supported themselves on their tube feet as untreated juveniles do, suggesting abnormal nervous

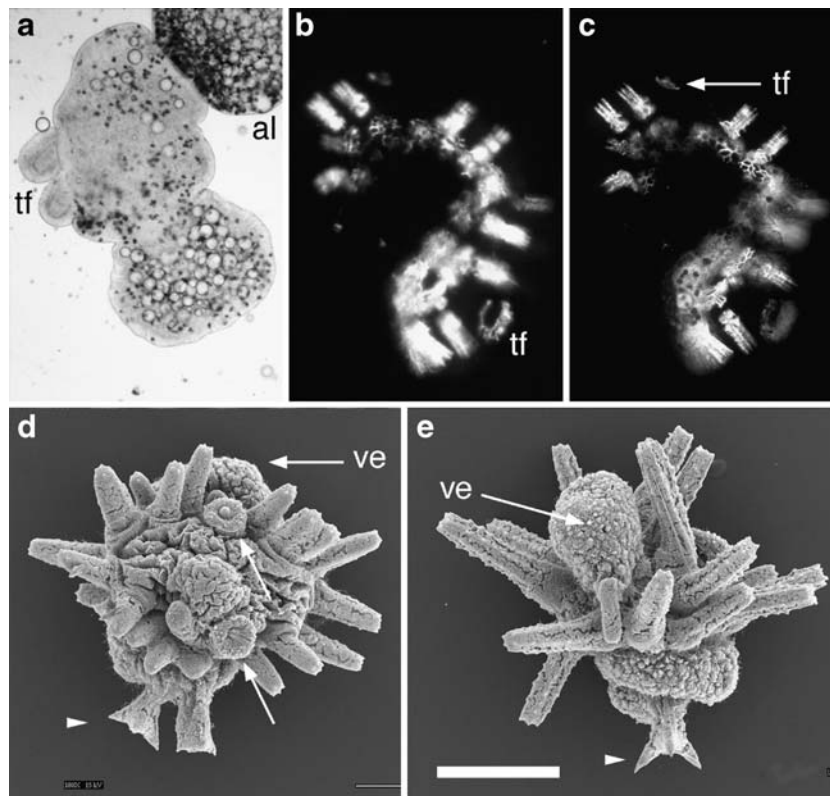


Fig. 4 Development of adult appendages and skeleton in NiCl₂-treated *H. erythrogramma* larvae. **a** 49-h larva viewed in bright field with two incipient tube foot buds developing from the middle of the larval midsection, together on one side of the larva. The vegetal lobe has already detached from this larva. **b** and **c** 3.5-day larva viewed under polarized light, photographed at two different focal planes; circumferential belt of spines is slightly oblique to the focal planes. The skeletal ring of one tube foot is in focus at the lower right in **b**. A second, smaller tube foot ring is seen on edge, in focus at the top of **c**. Note the distance between the two tube feet; they did not develop together as a cluster. Skeletons of several adult spine primordia are in focus in **c**. **d** and **e** Typical NiCl₂-treated larvae from spawning 1, at 4 days postfertilization, viewed by SEM. Animal and vegetal lobes have both detached, leaving only the larval midsection, covered in

vestibular ectoderm. The larval animal–vegetal axis is roughly vertical in both panels. **d** A category 1 larva showing two tube feet with mature suckers (arrows) surrounded by a large disorganized ring of adult spines on one side of the axis (compare to the orderly arrangement in Fig. 3). These obscure, in this view, the overall shape of the larva, which is similar to the one in **e**. Two juvenile spines (arrowhead) are located at one end. **e** A category 2 larva without any obvious cluster of appendages on one side of the axis. Instead, adult spines ring the axis circumferentially, restricted to the central belt. The ectoderm at the animal and vegetal ends is mostly unadorned with the exception of a well-developed juvenile spine at one end (arrowhead). This individual developed no tube feet. *al* animal lobe, *tf* tube feet, *ve* vestibular ectoderm. Bar=200 μm

system development. By 2.5 days, spine primordia began to appear (equivalent to untreated larvae diagrammed in Fig. 1c, d), developing normal spine skeletons (Fig. 4b, c) and growing to full length over about 2 days (Fig. 4d, e). Adult and juvenile spines were clearly distinguishable and normal in morphology (Fig. 4d, e). The normal appendage morphology reinforces our earlier conclusion (Minsuk and Raff 2005) that, at the low concentrations used in these experiments, NiCl₂ does not cause general, nonspecific physiological disruption, but instead acts through specific interference with axial patterning pathways.

Although the morphology of these appendages was normal, their distribution was abnormal. Most larvae developed one or two tube feet (Fig. 4), but some never developed any (Fig. 4e), and others developed as many as six. These often clustered on one side of the larva (Fig. 4a). In contrast to normal juveniles in which distinct pentaradial sets of spines appear in synchrony, spine primordia in sinistralized larvae were added gradually, reaching numbers comparable to or exceeding those in untreated controls. The appendages were arranged in distinct zones suggesting the presence of PD patterning, often with a central cluster suggesting a proximal pole. But within each zone, the CO appendage distribution was disordered with no indication of any periodic pattern, pentaradial or otherwise. The details of the appendage pattern were scored in specimens fixed at 4 days postfertilization from two separate spawnings (total $N=120$). These spawnings, although the same age, differed enough in the degree of appendage development that they must be described separately.

In spawning 1, appendage development was concentrated in the narrow middle of the vestibular hourglass with the wider animal and vegetal ends mostly bare (Fig. 4e). As a result, the main axis of the hourglass (the larval animal–vegetal axis) could be easily identified, and the positions of the various appendage regions could be scored relative to that axis. Of 40 specimens examined, 39 could be classified into one of three distinct categories. In category 1 ($N=13$, 32%), the adult spines formed a dense ring-shaped cluster on one side of the larva, its center located on one side of the narrow belt circling the middle of the hourglass (Fig. 4d). All tube feet present in these specimens were located just inside the inner edge of the ring of adult spines (Fig. 4d). In category 2 ($N=15$, 38%), the clustering was absent and the adult spines were distributed evenly along the narrow central belt of the hourglass, around the entire circumference (Fig. 4e), with the tube feet scattered among them (as in Fig. 4b, c, although these came from a different spawning). Category 3 larvae ($N=11$, 28%) displayed an intermediate morphology consisting of a composite of the features of categories 1 and 2: the ring-shaped cluster of adult spines and tube feet was present on one side and additional adult spines developed in a zone extending

circumferentially outward from the cluster along the central belt. These categories are diagrammed schematically in Fig. 8b–d, respectively, in which the green zone represents the location of adult spines. In all these variants, juvenile spines were sparse, with zero to four per specimen, restricted to the animal and vegetal regions of the vestibular ectoderm (Fig. 4d, e). Thus, distinct tiers of spines were aligned along the larval animal–vegetal axis (adult spines in the middle and juvenile spines at the two ends). In categories 1 and 3 (60% of the specimens scored in this spawning), the adult spines formed a ring that separated the tube feet inside the ring from the juvenile spines outside the ring, thereby making distinct concentric zones. This suggests that NiCl₂-treated larvae retain aspects of PD patterning, in contrast to their total lack of CO organization.

In spawning 2, as in spawning 1, CO organization was completely absent, whereas aspects of PD patterning appeared to be retained. However, development of both types of spines was much more extensive, perhaps reflecting temperature-induced between-spawning differences in developmental rate. Dense spines covered most or all of the surface, obscuring the hourglass shape of the specimens and the location of the animal–vegetal axis. We, therefore, evaluated the presence of PD patterning by assessing the positions of different appendage regions relative to one another. In 70 of 80 specimens examined, the surface was divided into distinct adult spine and juvenile spine regions, segregated by sharp boundaries. In most of the remaining ten cases, the arrangement was similar but the juvenile and adult spines were not neatly segregated. Tube feet, when present (72 of 80 specimens), were always located within the adult spine region, and of the 54 specimens bearing more than one tube foot, the tube feet were clustered together in 35 (65%), segregated from the surrounding adult spines. Thus, the appendage regions displayed a tiered, and usually clustered, arrangement, suggesting aspects of PD patterning as in spawning 1.

Unlike ectoderm, *H. erythrogramma* endoderm and mesoderm are not sinistralized by NiCl₂ treatment

The presence of apparent PD organization centered on a proximal pole, as described above, occurs on the left side of normal larvae and is, therefore, unexpected in a sinistralized context in which all sides of the larva are patterned as left side. This suggested that the sinistralization of the larva by NiCl₂ (Minsuk and Raff 2005) may affect the ectoderm alone, allowing the coelom to develop with normal asymmetry and provide an inductive signal to one side of the ectoderm, as in normal larvae (Minsuk and Raff 2002). We, therefore, examined mesoderm development in NiCl₂-treated embryos at late gastrula and early larval stages, when they first become distinguishable from normal embryos.

In untreated larvae, the development of the left coelom is the first morphological expression of left–right asymmetry. By 21.5 h, the left coelom has already formed at the tip of the gut, is quite a bit wider than the gut, and lies alongside it, extending from the gut tip nearly back to the vegetal pole (Fig. 5a–b). The vestibular ectoderm subsequently thickens and invaginates on the left side (Fig. 5c–d). In NiCl₂-treated larvae at the same times, the thickened, sinistralized vestibular ectoderm surrounded the circumference of the larva (Fig. 5g–h), whereas the gut and left coelom formed with normal morphology and asymmetry (Fig. 5e–h).

Mesoderm–ectoderm signaling in sinistralized embryos

In normal larvae, development of rudiment structures such as tube feet requires an inductive signal from the left coelom to the overlying ectoderm (the vestibule floor). An early response to this signal is the downregulation of *HeARS* expression in the vestibule floor, causing a gap in

the previously pan-ectodermal expression pattern (Fig. 6a) (Minsuk and Raff 2002). Because NiCl₂-treated embryos develop tube feet, we expected that the signal would be present and that the vestibular ectoderm would show the regulatory response. In order to verify that the response occurs and to determine the size, shape, and location of the responding region, we assayed *HeARS* expression in several sinistralized larvae (Fig. 6b, c). *HeARS* expression was present over the major portion of the vestibular ectoderm, but was absent in a relatively localized region overlying the coelom, on one side of the larval midsection. This is consistent with normal signaling, causing *HeARS* downregulation only in the region in contact with the coelom.

Late NiCl₂ treatments cause nonsinistralized larvae to produce sectorized juveniles with variable symmetry

Larval sensitivity to NiCl₂ declines after 10 h postfertilization and is undetectable after 16 h (Minsuk and Raff 2005).

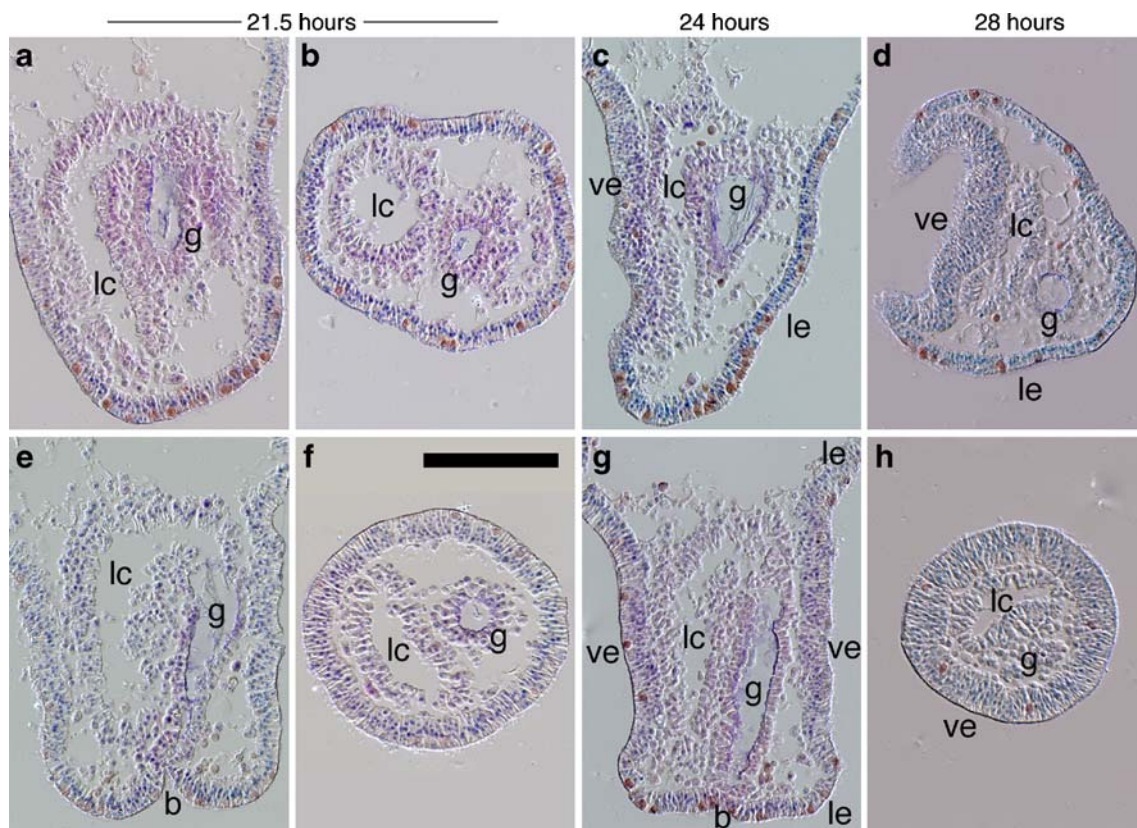


Fig. 5 Coelom development in untreated and NiCl₂-treated larvae. Paraffin sections. *Top row* untreated late gastrulae (21.5 h) and early larvae (24 and 28 h) with the larval left side to the *left* in all panels. **a** and **c** Frontal sections with vegetal pole at the bottom; **b** and **d** transverse sections. *Bottom row* NiCl₂-treated larvae at the same ages, oriented similarly (with respect to the axes indicated by the gut and coelom). In untreated larvae, coelomic mesoderm forms to the left side of the gut (**a–d**) and the vestibular ectoderm thickens and invaginates

on the left side (**c** and **d**). In NiCl₂-treated larvae, the vestibular ectoderm exhibits symmetrical, circumferential thickening (visible at the *left* and *right* in **g** and around the entire circumference in **h**) and the larva narrows as the ectoderm tries to invaginate everywhere (**g** and **h** are narrower than **e** and **f**). But the gut and coelom have normal, asymmetric morphology (compare those tissues in each panel in **e–h** to its pair in **a–d**). *b* blastopore, *g* gut, *lc* left coelom, *le* larval ectoderm, *ve* vestibular ectoderm. Bar=100 μm

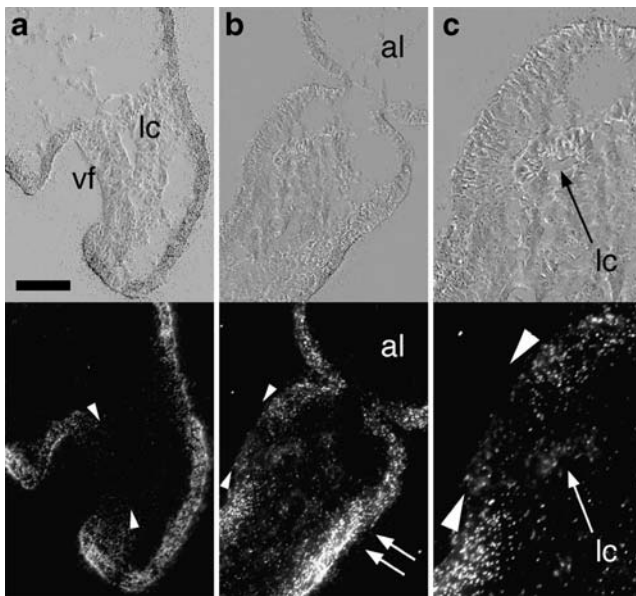


Fig. 6 Inductive signaling in untreated and NiCl_2 -treated larvae. Tissue morphology in DIC optics (*top row*) and *HeARS* expression pattern in dark field (*bottom row*). **a** Untreated larva, 28 h. **b** NiCl_2 -treated larva, 32 h. In both specimens, *HeARS* is downregulated (*arrowheads*) in the ectoderm overlying the coelom—the vestibule floor in **a** and a small nearby region on one side of the sinistralized ectoderm in **b**. The region of downregulation does not expand circumferentially in NiCl_2 -treated larvae; *HeARS* remains strongly expressed on the opposite side of the larva (*double arrow* in **b**). **c** Magnified view of **b** showing detail of left coelom and expression boundaries. *al* animal lobe, *lc* left coelom, *vf* vestibule floor. Bar=100 μm

We produced 151 mildly affected larvae by beginning treatment at 13–15 h postfertilization. Of these, 143 had perfectly normal morphology, or nearly so, producing more or less normally invaginating vestibules, which everted at metamorphosis to produce a spheroidal juvenile in the normal fashion, in contrast to the hourglass-shaped “juveniles” formed on the exposed vestibular ectoderm of fully sinistralized larvae. The appendage patterns were scored in 80 of the emerging juveniles. Some of these were severely affected, resembling the juveniles of sinistralized larvae, but the majority (53) were much better organized, possessing well-defined CO sectors indicated by a proximal zone of tube feet alternating with adult spine triplets and a distal zone of juvenile spine pairs aligned with the tube feet, as in normal juveniles. However, these juveniles ranged from biradial to decaradial (Table 1, Fig. 7). (They also suffered from various individual appendage abnormalities including duplications (Fig. 7), deletions, and replacement of an adult

spine by a juvenile spine or vice versa.) Thus, NiCl_2 disrupts CO patterning in a quantitative rather than an all-or-nothing manner.

Discussion

Earlier studies have shown that ray number, and thus CO patterning, can be disturbed by environmental or genetic factors. We know of no studies investigating PD patterning. High salinity was found to induce normally five-armed starfish species to develop three or four arms (Watts et al. 1983; Marsh et al. 1986). Hinegardner (1975) observed symmetry disruption in inbred lines of the indirect-developing sea urchin *Lytechinus pictus*, similar to the variable symmetry we obtained using late NiCl_2 treatment. These lines produced adult urchins with two to six rays, demonstrating that there is a genetic basis for symmetry regulation. However, none of these studies addressed the mechanisms underlying axial patterning. In contrast to earlier studies, we have addressed these mechanisms by examining the development of the vestibule and left coelom (instead of just juvenile morphology); by investigating finer elements of the adult pattern (CO and PD elements of appendage patterning instead of just ray number); by using a method that targets a specific germ layer, the ectoderm, thus allowing us to tease apart the roles of the germ layers in normal patterning; and by demonstrating a timing-dependent effect (abolishment of CO patterning vs. symmetry disruption).

Distinct circumoral and proximodistal modules pattern the normal adult body plan

The appendage pattern in fully sinistralized, NiCl_2 -treated larvae retains some but not all elements of normal juvenile/adult pattern. The sectorized organization of normal pentamery never forms in these larvae and the CO arrangement of appendages is disordered. But tube feet, adult spines, and juvenile spines are generally restricted each to their own concentric zones on the surface of the larval midsection (Fig. 4d), recalling, albeit imperfectly, the organization of these elements in normal juveniles (Fig. 3c). If we assume that each zone of appendages represents a distinct ectodermal territory with its own positional identity, then we can map out the correspondence between the ectodermal territories of normal juveniles and those of NiCl_2 -treated

Table 1 Distribution of symmetries in radially symmetrical juveniles after late NiCl_2 treatment

Number of rays	2	3	4	5	6	7	8	9	10	Total	Total nonpentaradial
Number of specimens	9	8	8	20	3	3	1	0	1	53	33 (62%)

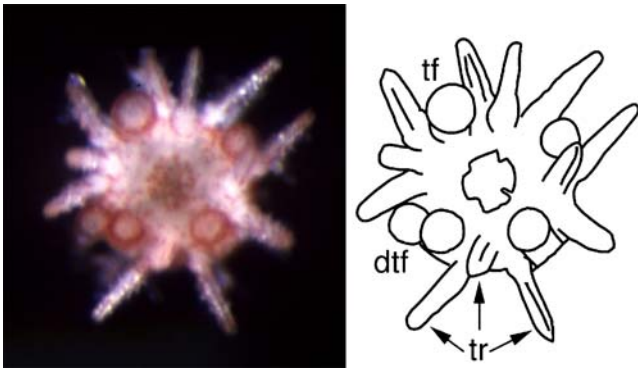


Fig. 7 Juvenile symmetry disruption in the absence of larval defects. Oral view of a 6-day-old juvenile derived from a late NiCl_2 -treated larva. The larvae had normal external morphology and underwent normal metamorphosis; the juvenile shows tetra-radial symmetry. A tracing of the major features of the juvenile is shown. Note the four adult spine triplets (*tr*) with the tube feet (*tf*) interposed between them at the corners of a square. One of the corners has two tube feet (*dff* duplicated tube foot), and the pattern of juvenile spines (out of the plane of focus and mostly hidden in this view) matched that of the tube feet with a duplication in the same corner, suggesting a tetra-radial repatterning combined with secondary duplication of structures along one radius

larvae. In normal juveniles, the adult spines are more proximal and the juvenile spines are more distal; the proximal pole, from which the PD axes diverge, is at the coelomic signaling center and site of future mouth formation, around which the concentric zones are arranged (Fig. 8a). By analogy, in sinistralized larvae, the proximal pole can be found at the center of the rings of adult spines (in spawning 1, categories 1 and 3) or of the tube foot clusters (in spawning 2), so that the path outward from the pole passes through the tube foot zone first, followed by the adult spine zone, and finally through the juvenile spine zone(s) most distally (Fig. 8b, d). In untreated juveniles, the remnant of the V/L boundary lies within the juvenile spine zone, at the aboral end of the OA axis (see Fig. 1). In a NiCl_2 -treated, sinistralized larva, there are two such boundaries, and they also lie within the juvenile spine zone, at the animal and vegetal lobe detachment points; thus they represent two separate aboral “poles” (Fig. 8b), and indeed, juvenile spines occur at either or both ends of the larva but not in the narrow central belt. These patterns suggest that although NiCl_2 treatment abolishes CO patterning, it does not abolish PD patterning. These then represent two modular pathways of adult development, at least partially independent, whose expression can be dissociated by such treatment.

The later treatment of embryos after the decline of NiCl_2 sensitivity resulted in the production of juveniles with less severe patterning defects. These juveniles had identifiable sectors as in normal juveniles, but the number of sectors varied. Therefore, CO patterning was not abolished, but its

quantitative regulation was disrupted. Therefore, NiCl_2 treatment does not simply impose an all-or-nothing block against CO patterning, but exerts finer influence as a function of timing. In these more mildly affected juveniles, PD patterning was normal, reinforcing the conclusion that PD and CO patterning are dissociable.

Interpreting the concentric patterns in fully sinistralized larvae as PD sequences implies that the tube feet and adult spines (red and green, respectively, in Fig. 8) represent sequential PD positional identities. However, these structures in normal juveniles are located side by side at a single PD position, in an alternating periodic pattern (Fig. 3). One way to account for this apparent contradiction is to hypothesize that the two structures are indeed patterned along the PD axes, but that in normal rudiments the zonal boundary undergoes a morphogenetic rearrangement producing the observed appendage pattern. Figure 8a illustrates a possible interpretation of the normal appendage pattern consistent with such a process, indicating a PD arrangement of the zones but allowing for a periodic CO arrangement of the tube feet and adult spines in their final positions.

This interpretation leads to several predictions. First, we expect that there should be two independent axial patterning pathways in the early rudiment, prior to the development of pentamer morphology. One, acting along the PD axes, would produce concentric gene expression territories, such as the restriction of *HeARS* to the aboral pole (the vestibule roof) as shown above (Minsuk and Raff 2002). We predict that other such markers exist, including some restricted to the oral region (vestibule floor) or with other concentric boundaries. A second, CO, pathway would be deployed perpendicular to the PD axes and should produce radial stripes representing the periodic patterning of the sectors. No such radial markers have been identified prior to the development of morphological pentamery, although gene expression patterns reflecting these expectations do arise later, after pentamer pattern and morphology have been established (Lowe and Wray 1997; Ferkowicz and Raff 2001; Lowe et al. 2002; Sly et al. 2002; Nielsen et al. 2003; Morris and Byrne 2005; Wilson et al. 2005).

Under such a scheme, the intersection of gene expression territories in concentric bands and radial stripes would be predicted to result in a pattern of tube foot and adult spine territories that are segregated along both axes. Morphogenetic movements would be required to bring the two sets of appendages into register within a single band. The absence of CO patterning information in NiCl_2 -treated larvae would likely disrupt such movements, leading the two bands to remain segregated, as we observed. In fact, exactly such morphogenetic movements were previously suggested by an independent line of evidence (Minsuk and Raff 2002). As a normal rudiment develops, the simple early *HeARS* expression pattern (subdividing the vestibule into two

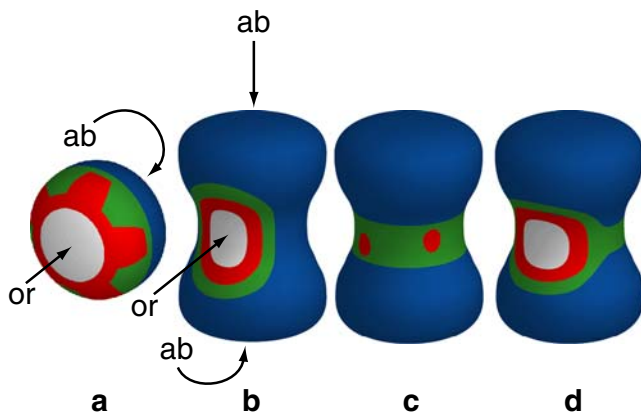


Fig. 8 Schematic representation of corresponding regions of positional identity in untreated and NiCl_2 -treated specimens. **a** Untreated juvenile **b–d** NiCl_2 -treated larvae, corresponding to the three pattern categories in spawning 1. *Blue* juvenile spine zone, *green* adult spine zone, *red* tube foot zone (or isolated individual tube feet in **c**), *ab* aboral, *or* oral. See text for further explanation

regions, proximal and distal) is transformed into a more complex pattern. We proposed that the pattern could be explained by the movement of *HeARS*-expressing spine ectoderm between nonexpressing early tube foot ectoderm from a more peripheral position, consistent with the pattern formation scheme suggested above.

CO patterning is ectoderm-dependent

NiCl_2 -treated, sinistralized larvae contain morphologically normal gut and left coelom. We cannot rule out cryptic defects, but the downregulation of *HeARS* in the overlying ectoderm, followed by appendage development, shows that the coelom can signal normally because these events depend on coelomic signaling (Minsuk and Raff 2002). Therefore, the disruption of CO patterning in both ectodermal and mesodermal germ layers by NiCl_2 treatment is unlikely to be mediated by coelomic mesoderm, and instead is likely to be ectoderm-dependent, as is the sinistralization of the larval ectoderm (Minsuk and Raff 2005).

This suggests that CO patterning of the mesoderm is dependent upon events taking place in the ectoderm. This may involve no more than a permissive signal, triggering CO patterning events in the mesoderm. Alternatively, the ectoderm may acquire pentamery first, and subsequently impart this pattern to the mesoderm via local signals. We favor the latter possibility because it better explains the production of sectored but nonpentameral juveniles by late NiCl_2 -treatment. Disruption of a simple permissive signal would be more likely to produce an all-or-nothing block to CO patterning.

Morphologically, pentamery appears in the mesoderm (the five hydrocoel lobes) earlier than in the ectoderm

(Ferkowicz and Raff 2001). If our interpretation is correct, then an inherent pentamery should already be present in the ectoderm prior to hydrocoel lobe formation. We, therefore, predict that pentamery will be found in ectodermal gene expression patterns well before it is morphologically expressed in either germ layer.

PD patterning is ectoderm- and mesoderm-dependent

By similar reasoning, PD patterning is likely to be mesoderm-dependent. In contrast to the NiCl_2 sensitivity of CO patterning, the concentric arrangement of appendage zones even in completely sinistralized larvae suggests that PD patterning is regulated, at least partly, by an independent, non- NiCl_2 -sensitive mechanism. Coelomic signaling is one immediately obvious candidate. We already know that a coelomic signal is required for the induction of adult ectodermal development (Minsuk and Raff 2002). In NiCl_2 -treated larvae, both the coelom and the signal are normal, and the ectoderm responds to the signal locally. This suggests that this same signal may organize the PD pattern, either directly, or indirectly by inducing an ectodermal signaling center.

However, the observed appendage patterns also provide evidence for additional PD control mechanisms, sensitive to NiCl_2 and thus probably ectodermal. Some larvae (spawning 1, category 1) display a simple clustered appendage pattern (Fig. 8b), but in many treated larvae (spawning 1, category 3), adult spines are distributed around a circumferential belt beyond the clustered “left side” (Fig. 8d), and in extreme cases (spawning 1, category 2), this feature dominates the morphology, resulting in a completely circumferential appendage pattern with no evidence of clustering at all (Fig. 8c). Because coelomic signaling appears to be normal and local, control of PD pattern by coelomic signaling alone should always produce the pattern in Fig. 8b, and therefore, cannot fully explain the observed range of results. It is possible that further in situ hybridization experiments may show greater variation with some individuals responding to the signal over a wider field. The basal surface of the vestibule apposed to the coelom is convex in normal larvae (Fig. 5d), but concave in sinistralized larvae (Fig. 5h), which increases the area of contact between the two tissues. But this would not likely produce patterns as extreme as that in Fig. 8c, given the normal coelomic morphology we see. Coelomic signaling combined with a second, NiCl_2 -sensitive ectodermal signal offers a better explanation. We suggest two alternative schemes.

First, an independent ectodermal signaling center could directly overlie a coelomic one. These could normally act additively as an organizer of the PD axes. If the ectodermal component were expanded around the larval circumference

in response to NiCl₂ treatment, it would tend to promote the pattern of Fig. 8c, whereas a non-NiCl₂-sensitive coelomic signal would promote the pattern of Fig. 8b. In combination, they should produce the pattern of Fig. 8d.

Alternatively, an ectodermal signaling center could be located aborally (distally), at the V/L boundary, rather than orally (proximally), and function antagonistically. Aboral signaling centers at the two V/L boundaries of NiCl₂-treated larvae, antagonistic to an oral, coelomic signaling center in the middle of one side, could generate the pattern of Fig. 8d. In either scenario, variation in relative strength of the component signals could explain the observed range of results.

Individual appendage patterning is non-NiCl₂-sensitive and locally controlled

Although the arrangement of appendages is disturbed by NiCl₂, individual appendage morphology is strikingly normal. Global pattern disruption, therefore, has no apparent effect on patterning or differentiation within each appendage. In contrast, the surgical removal of left coelom (Minsuk and Raff 2002) severely impaired the development not only of tube feet (containing coelomic derivatives), but also of spines (with no coelomic component). The few individual skeletal elements that did develop in the absence of coelom were poorly formed, so the impairment was not restricted to global patterning but affected local interactions. We concluded that coelomic signals pattern the mesenchyme in adult skeleton, either directly or by inducing an intermediary ectodermal signal. Production of normal appendages in the abnormal arrangement of a NiCl₂-treated larva implies the coordinated local morphogenesis of ectoderm, coelom, and mesenchyme, suggesting extensive signaling between these components, unperturbed by NiCl₂ (or by the resulting sinistralized vestibular phenotype) but requiring the presence of coelom. If PD patterning is coelom-dependent as we suggest, it may be a critical element underlying the patterning of individual appendages.

Pattern vs. patterning: the origin of radial symmetry

The distinct pentaradial symmetry of the adult echinoderm does not automatically demand an equally symmetric patterning process. We have suggested that CO patterning may be controlled by the ectoderm, but we cannot yet say what kind of event provides the positional information to determine the identities of the territories and structures that arise at different positions around the ring. The simple appendage pattern of juveniles suggests a simple symmetrical ring with no endpoint—a circular axis without any identifiable poles—which must be divided into periodic sectors. This impression is reinforced by gene expression patterns within

the juvenile central nervous system, which are uniformly pentaradial with no hint of endpoints (Sly et al. 2002).

Alternatively, a circular pattern could arise from a more traditional linear axis that has been wrapped into a circle, bringing the ends into proximity; the circle would then have a natural internal breakpoint and real poles. The hydrocoel progresses from a simple pouch to a ring-shaped tube. In some echinoderm species, the ring may arise by the perforation of the center of the pouch (Bury 1889; MacBride 1903; and our unpublished observations on *H. erythrogramma*), but in others, the original pouch lengthens into a tube and bends until its ends meet and fuse, forming a ring (Bury 1889; Okazaki 1975; Smiley 1986; Hendlar 1991; Smiley et al. 1991). In these species, therefore, the circle has endpoints, and each of the five hydrocoel lobes has a unique position between the endpoints. Several authors have suggested—based on living and fossil adult morphology, on larval gene expression patterns, or on comparative embryology—that the individual rays form a linear sequence, with a central ray representing the adult anterior (Paul and Smith 1984; Hotchkiss 1998), posterior (Morris 1999), or ventral (Peterson et al. 2000), flanked by two lateral pairs of rays, left and right. The question thus arises, whether pentamery is patterned along a continuous circle or along a curved axis with endpoints, and where those endpoints, if any, are located.

This question is closely related to the question of axial homologies of echinoderms to other bilaterians, a controversial and unresolved topic. It has been variously suggested that the individual rays represent duplicated bilaterian anterior–posterior (AP) axes (Raff 1996; Raff and Popodi 1996; Wray 1998) or that they are homologous to bilaterian appendages (Hotchkiss 1998; Morris 1999) with the homologue of bilaterian AP lying either along the echinoderm adult OA axis (David and Mooi 1998; Peterson et al. 2000) or along the curve of the radial water canal and the nerve ring (Raff 1996; Raff and Popodi 1996; Morris 1999).

Attempts to resolve these issues have been further complicated by the confusion between the OA and PD axes of sea urchins, which we have attempted to clarify. For example, Morris and Byrne (2005) examined the conserved axial patterning genes *Hox11/13*, *Hox5*, and *orthodenticle* in the direct-developing sea urchin *Holopneustes purpureus* and found them expressed in a linear sequence, just as they are in the bilaterian AP axis. All three were expressed in the vestibular ectoderm with *Hox11/13* in the most distal part, *orthodenticle* in the most proximal part (the central nerve ring), and *Hox5* between them. This pattern was interpreted as an aboral-to-oral sequence, and therefore, as consistent with homology between bilaterian AP and echinoderm OA. This exemplifies the problem caused by the highly derived, seemingly OA orientation of sea urchin rays. Any discussion of echinoderm/bilaterian homologies must make sense in the

light of the common body plan of echinoderms in which, as we have emphasized (Fig. 2), the rays must be seen as separate PD axes, perpendicular to the OA axis. With this framework in mind, the gene expression pattern of Morris and Byrne (2005) is not aligned along the OA axis, but along the PD axes.

Bilateria axial homologies remain a perplexing problem, obscured by the body plan transformations that have occurred during echinoderm evolution (Minsuk et al. 2005; Smith 2008). We have begun to distinguish the roles of the interacting germ layers in establishing the body plan, opening the possibility that these processes may help to illuminate echinoderm–bilateria homologies and the competing theories of echinoderm body plan evolution.

Acknowledgments We thank the Sydney Aquarium and the School of Biological Sciences, University of Sydney for providing resources and for making our work in Australia possible; Gerd Müller and Wolfgang Weninger for the use of equipment; Meg Snoko for help with specimen treatment and transport; and Ulrich Krohs and Ellen Popodi for helpful discussion. We would also like to thank the anonymous reviewers for comments on the manuscript and Javier Capdevila for comments on an earlier draft. New South Wales Fisheries provided collection permits. This work was funded by an NIH Postdoctoral Fellowship to SBM and an NSF research grant to RAR.

References

- Aihara M, Amemiya S (2001) Left–right positioning of the adult rudiment in sea urchin larvae is directed by the right side. *Development* 128:4935–4948
- Angerer LM, Angerer RC (1991) Localization of mRNAs by in situ hybridization. *Methods Cell Biol* 35:37–71
- Bury H (1889) Studies in the embryology of the echinoderms. *Q J Microsc Sci* 29:409–447 (+plates 37–39)
- David B, Mooi R (1998) Major events in the evolution of echinoderms viewed by the light of embryology. In: Mooi R, Telford M (eds) *Echinoderms*. San Francisco. Balkema, Rotterdam, pp 21–28
- Duboc V, Röttinger E, Lapraz F, Besnardeau L, Lepage T (2005) Left–right asymmetry in the sea urchin embryo is regulated by Nodal signaling on the right side. *Developmental Cell* 9:147–158
- Emler RB (1995) Larval spicules, cilia, and symmetry as remnants of indirect development in the direct developing sea urchin *Heliocidaris erythrogramma*. *Dev Biol* 167:405–415
- Ferkowicz MJ, Raff RA (2001) Wnt gene expression in sea urchin development: heterochronies associated with the evolution of developmental mode. *Evol Dev* 3:24–33
- Haag ES, Raff RA (1998) Isolation and characterization of three mRNAs enriched in embryos of the direct-developing sea urchin *Heliocidaris erythrogramma*: evolution of larval ectoderm. *Dev Genes Evol* 208:188–204
- Hadfield MG (1975) Hemichordata. In: Giese AC, Pearse JS (eds) *Reproduction of marine invertebrates*, vol 2. Entoprocts and lesser coelomates. Academic, New York, pp 185–240
- Hardin J, Coffman JA, Black SD, McClay DR (1992) Commitment along the dorsoventral axis of the sea urchin embryo is altered in response to NiCl₂. *Development* 116:671–685
- Hendler G (1991) Echinodermata: ophiuroidea. In: Giese AC, Pearse JS, Pearse VB (eds) *Reproduction of marine invertebrates*, vol 6. Echinoderms and lophophorates. Boxwood, Pacific Grove, CA, pp 355–511
- Hinegardner RT (1975) Morphology and genetics of sea urchin development. *Am Zool* 15:679–689
- Hotchkiss FHC (1998) A “rays-as-appendages” model for the origin of pentamerism in echinoderms. *Paleobiology* 24:200–214
- Hyman LH (1955) *The invertebrates*, vol. 4. Echinodermata. McGraw-Hill, New York
- Hyman LH (1959) *The Invertebrates*. vol. 5. Smaller coelomate groups. McGraw-Hill, New York
- Lowe CJ, Wray GA (1997) Radical alterations in the roles of homeobox genes during echinoderm evolution. *Nature* 389:718–721
- Lowe CJ, Issel-Tarver L, Wray GA (2002) Gene expression and larval evolution: changing roles of *distal-less* and *orthodenticle* in echinoderm larvae. *Evol Dev* 4:111–123
- MacBride EW (1903) The development of *Echinus esculentus*, together with some points in the development of *E. miliaris* and *E. acutus*. *Phil Trans R Soc Lond B* 195:285–327 (+plates 7–16)
- Marsh AG, Watts SA, Chen CP, McClintock JB (1986) The effect of high salinity on development, mortality and ray number of *Echinaster spinulosus* (Echinodermata: Asteroidea) at different developmental stages. *Comp Biochem Physiol* 83A:229–231
- McCain ER, McClay DR (1994) The establishment of bilateral asymmetry in sea urchin embryos. *Development* 120:395–404
- Minsuk SB, Raff RA (2002) Pattern formation in a pentamerous animal: induction of early adult rudiment development in sea urchins. *Dev Biol* 247:335–350
- Minsuk SB, Raff RA (2005) Co-option of an oral-aboral patterning mechanism to control left–right differentiation: the direct-developing sea urchin *Heliocidaris erythrogramma* is sinistralized, not ventralized, by NiCl₂. *Evol Dev* 7:289–300
- Minsuk SB, Andrews ME, Raff RA (2005) From larval bodies to adult body plans: patterning the development of the presumptive adult ectoderm in the sea urchin larva. *Dev Genes Evol* 215:383–392
- Morris VB (1999) Bilateral homologues in echinoderms and a predictive model of the bilateral echinoderm ancestor. *Biol J Linn Soc* 66:293–303
- Morris VB, Byrne M (2005) Involvement of two Hox genes and *Otx* in echinoderm body-plan morphogenesis in the sea urchin *Holopneustes purpurescens*. *J Exp Zool B Mol Dev Evol* 304B:456–467
- Nielsen MG, Popodi E, Minsuk S, Raff RA (2003) Evolutionary convergence in *Otx* expression in the pentamerous adult rudiment in direct-developing sea urchins. *Dev Genes Evol* 213:73–82
- Okazaki K (1975) Normal development to metamorphosis. In: Czihak G (ed) *The sea urchin embryo*. Springer, New York, pp 177–232
- Paul CRC, Smith AB (1984) The early radiation and phylogeny of echinoderms. *Biol Rev* 59:443–481
- Peterson KJ, Cameron RA, Tagawa K, Satoh N, Davidson EH (1999) A comparative molecular approach to mesodermal patterning in basal deuterostomes: the expression pattern of *Brachyury* in the enteropneust hemichordate *Ptychodera flava*. *Development* 126:85–95
- Peterson KJ, Arenas-Mena C, Davidson EH (2000) The A/P axis in echinoderm ontogeny and evolution: evidence from fossils and molecules. *Evol Dev* 2:93–101
- Raff RA (1996) *The shape of life*. The University of Chicago Press, Chicago

- Raff RA, Popodi EM (1996) Evolutionary approaches to analyzing development. In: Ferraris JD, Palumbi SR (eds) Molecular zoology: advances, strategies, and protocols. Wiley, New York, pp 245–265
- Sly BJ, Hazel JC, Popodi EM, Raff RA (2002) Patterns of gene expression in the developing adult sea urchin central nervous system reveal multiple domains and deep-seated neural pentamerism. *Evol Dev* 4:189–204
- Smiley S (1986) Metamorphosis of *Stichopus californicus* (Echinodermata: holothuroidea) and its phylogenetic implications. *Biol Bull* 171:611–631
- Smiley S, McEuen FS, Chafee C, Krishnan S (1991) Echinodermata: holothuroidea. In: Giese AC, Pearse JS, Pearse VB (eds) Reproduction of marine invertebrates, vol 6. Echinoderms and lophophorates. Boxwood, Pacific Grove, CA, pp 663–750
- Smith AB (2008) Deuterostomes in a twist: the origins of a radical new body plan. *Evol Dev* 10:493–503
- Summers RG, Piston DW, Harris KM, Morrill JB (1996) The orientation of first cleavage in the sea urchin embryo, *Lytechinus variegatus*, does not specify the axes of bilateral symmetry. *Dev Biol* 175:177–183
- Urata M, Yamaguchi M (2004) The development of the enteropneust hemichordate *Balanoglossus misakiensis* Kuwano. *Zool Sci* 21:533–540
- Watts SA, Scheibling RE, Marsh AG, McClintock JB (1983) Induction of aberrant ray numbers in *Echinaster* sp. (Echinodermata: Asteroidea) by high salinity. *Fla Sci* 46:125–128
- Williams DHC, Anderson DT (1975) The reproductive system, embryonic development, larval development and metamorphosis of the sea urchin *Heliocidaris erythrogramma* (Val.) (Echinoidea: Echinometridae). *Aust J Zool* 23:371–403
- Wilson KA, Andrews ME, Raff RA (2005) Dissociation of expression patterns of homeodomain transcription factors in the evolution of developmental mode in the sea urchins *Heliocidaris tuberculata* and *H. erythrogramma*. *Evol Dev* 7:401–415
- Wray GA (1998) Origin and diversification of echinoderm body architecture: insights from the expression of body-patterning genes. In: Mooi R, Telford M (eds) Echinoderms: San Francisco. Balkema, Rotterdam, p 90